International Journal on Magnetic Particle Imaging
Vol 3, No 2, Article ID 1707004, 10 Pages

Infinite Science Publishing

Research Article

Model uncertainty in magnetic particle imaging: Nonlinear problem formulation and model-based sparse reconstruction

Tobias Kluth[a,*] · Peter Maass[a]

[a]Center for Industrial Mathematics, University of Bremen, Bremen, Germany
[*]Corresponding author, email: tkluth@math.uni-bremen.de

Received 25 November 2016; Accepted 18 June 2017; Published online 28 July 2017

Abstract

In magnetic particle imaging the concentration of superparamagnetic iron oxide nanoparticles is determined by measuring the particle's nonlinear response to an applied magnetic field. The particles are highly sensitive to the dynamic magnetic field which allows a rapid data acquisition. As a result magnetic particle imaging benefits from a high temporal resolution and can reach high spatial resolutions. But model-based reconstruction techniques are still not able to reach the quality of data-based approaches. In the latter case the linear system function is determined by a time-consuming measurement process which also has negative implications for the spatial resolution of the reconstructions. Common model approaches are overly simplified leading to reconstructions of minor quality. We aim for the formulation of a nonlinear parameter identification problem which is able to deal with model errors while reconstructing a sparse concentration. For this purpose we use a total least squares approach to simultaneously reconstruct the tracer concentration and deviations in the system matrix. The starting point is a commonly used model which is investigated with respect to the simplifying assumptions to derive a formal definition of the problem. Sparsity constraints are introduced for the concentration function and reconstructions are obtained from publicly available data by minimizing a Tikhonov-type functional. Data-based as well as model-based reconstructions are computed and improved by using the total least squares approach.

I. Introduction

In magnetic particle imaging (MPI) the behavior of superparamagnetic iron oxide nanoparticles is used to reconstruct the concentration of particles [1]. The particle's nonlinear response to the applied dynamic magnetic field is measured in multiple receive coils. These signals are used to compute an image reconstruction. A high temporal resolution and a potentially high spatial resolution make MPI suitable for several in-vivo applications. For example, imaging blood flow or tracking medical instruments [2–4] are possible applications of MPI without the need for harmful radiation. Both applications benefit from the fast data acquisition of MPI but also require computationally efficient reconstruction methods to allow real time observations. Mathematical models are advantageous for the development of methods which fulfill the latter requirement.

In good approximation the relationship between particle concentration and measured potential is modeled by a Fredholm integral equation of the first kind. For some tracers a nonlinear dependence on the concentration is reported for large concentrations [5]. As the affected concentrations are larger than the concentra-

tions commonly used in MPI experiments, these effects are not included in existing models used for imaging. The challenging part of modeling MPI appropriately is finding the correct integral kernel, respectively system function, which describes the particle behavior. Existing model-based reconstructions incorporate particle behavior based on the theory of paramagnetism. This model was recently analyzed more theoretically in the context of MPI [6]. Methods based on ideal magnetic fields [7, 8] and on realistic magnetic fields [9] are promising but they are not able to reach the quality of measured system functions. One possible reason is the particle relaxation which arouses increasing interest in MPI. Ordinary differential equations are combined with the paramagnetic particle behavior [10] to deal with this issue. The properties of more complicated relaxation models are also investigated with respect to the particle's behavior. In particular, relaxation in magnetic fields which are commonly used in MPI is of interest [11] but have not been applied to the imaging problem. Relaxation effects are likely to emerge in magnetic fields belonging to MPI sequences since they are generated by moving the field free point (FFP) along a given trajectory rapidly.

In case of a Lissajous trajectory the system matrix obeys a complex structure. In absence of suitable models the matrix is usually measured [12, 13] in a time-consuming measurement process where a "delta" probe is moved through the field of view. In contrast, Cartesian sequences [10, 14, 15] allow modeling the MPI signal by a spatial convolution. Reconstruction methods based on these sequences are used to obtain x-space reconstructions [8, 16].

The considered reconstruction in MPI is a linear ill-posed inverse problem [6, 17] which is solved by applying Tikhonov regularization [2, 18–20]. Due to the complexity, the use of iterative solvers is advantageous. In the literature the problem is solved preferably by using the algebraic reconstruction technique [2, 18, 21, 22] combined with a nonnegativity constraint [2]. The Kaczmarz method shows fast convergence due to the fact that the rows of the system matrix are close to orthogonal. Tikhonov regularization was applied to both kinds of system functions, data-based as well as model-based. Regularization techniques like fused lasso regularization or other gradient-based methods were recently applied to the data-based MPI problem [14, 23]. Directional total variation was also applied to the MPI problem in a simulation study [24]. But model-based approaches have not been investigated with respect to regularization techniques like introducing, for example, a sparsity term [25] or a total variation term [26].

However, it is still an open challenge to deal with the uncertainties in the MPI model. The potential of methods dealing with measurement errors in the system matrix, e.g., total least squares [27], was already mentioned [20]. But these methods have neither been applied to the data-based nor to the model-based MPI problem. Furthermore, the identification of a suitable mathematical model for MPI which describes the system's behavior for different kinds of FFP trajectories is still an unsolved problem.

In this work, we investigate an existing model approach with respect to potential model errors. Based on that knowledge we formulate a nonlinear problem to compensate for these model uncertainties. Our goals are the following: (1) building a formal framework to define the model assumptions and the resulting problem; (2) introducing a sparsity constraint for the particle concentration; (3) a nonlinear problem formulation based on the total least squares approach considering errors in the system matrix; and (4) first numerical comparison of data-based and model-based reconstructions with sparsity constraints with and without taking errors in the system matrix into account.

The paper is organized as follows. In Sec. II, the model-based MPI forward operator is first derived and the model assumptions are identified. Moreover, sparsity constraints are introduced for the discretized problem. The Tikhonov functional is minimized by an iterated soft shrinkage algorithm. Then the problem is extended to a nonlinear problem based on the total least squares approach. Finally, data-based and model-based approaches are investigated with respect to publicly available real data in Sec. III. The paper concludes with a discussion in Sec. IV.

II. Methods

II.I. Model

Due to the ill-posed nature of the problem, the reconstruction is highly sensitive to measurement errors or potential model errors. We thus review a commonly used physical model for reconstructions with Cartesian-type and Lissajous-type FFP trajectories to clearly identify the assumptions in the mathematical model. For this purpose we follow the formal considerations in [6, 28]. Note that the present model was already used in earlier works, e.g., in [7, 8, 16].

The main focus in magnetic particle imaging is determining a spatial concentration distribution of the injected nanoparticles. These nanoparticles are assumed to be spatially distributed in a field of view which is given by the open, bounded, and connected set $\Omega \subset \mathbb{R}^d$, $d = 1, 2, 3$. The concentration of nanoparticles is thus a scalar function which is real-valued and nonnegative, i.e., the concentration is given by a function $c : \mathbb{R}^d \to \mathbb{R}$ with $c(\mathbf{x}) \geq 0$, $\forall \mathbf{x} \in \Omega$, and $\operatorname{supp}(c) \subset \Omega$ (A1).

We will further consider the following four components: the measured signal $\mathbf{v}$, the induced signal $\mathbf{u}$ in the receive coils, the applied magnetic field $\mathbf{H}$,

10.18416/ijmpi.2017.1707004

and the particle magnetization $\mathbf{M}$. The measured signal is a time-dependent real-valued potential function $\mathbf{v}:(0,T)\to\mathbb{R}^L$, $L\in\mathbb{N}$, and $0<T<\infty$. Each element of $\mathbf{v}$ corresponds to one of the L receive coils. $\mathbf{v}$ is not exactly the induced signal $\mathbf{u}:(0,T)\to\mathbb{R}^L$ in the receive coils. Due to an analog filter process, which is implemented to remove the excitation signal, a filtered version of the induced signal is measured. It is assumed that this analog filter can be formulated by a temporal convolution operation with given kernels $a_k:\mathbb{R}\to\mathbb{R}$, $k=1,\dots,L$. The transfer functions are often assumed to be ideal band pass filters which remove the excitation signal from the induced potential (A2). Alternatively, the transfer function is fitted to the measured system function [12]. However, the resulting signal $\mathbf{v}$ is then given by

$$v_k(t)=(a_k*u_k)(t),\ t\in(0,T),\ k=1,\dots,L, \tag{1}$$

where u_k is the induced potential in the k-th receive coil. The vector function $\mathbf{u}$ is given by the temporal change of the magnetic flux $\mathbf{\Phi}:(0,T)\to\mathbb{R}^L$. From Faraday's law of induction follows

$$\mathbf{u}(t)=-\frac{d}{dt}\mathbf{\Phi}(t). \tag{2}$$

The magnetic flux is given by the law of reciprocity [29] which relates the magnetic flux to a volume integral, i.e.,

$$\mathbf{\Phi}(t)=\mu_0\int_{\mathbb{R}^d}\mathbf{p}_\mathrm{R}(\mathbf{x})^T(\mathbf{M}(\mathbf{x},t)+\mathbf{H}(\mathbf{x},t))\,d\mathbf{x}, \tag{3}$$

where $\mathbf{p}_\mathrm{R}:\mathbb{R}^d\to\mathbb{R}^{d\times L}$ contains the coil sensitivity of each receive coil in the columns and μ_0 is the magnetic permeability in vacuum. The magnetic flux comprises two signals. One is induced by the magnetic field $\mathbf{H}:\mathbb{R}^d\times(0,T)\to\mathbb{R}^d$ and the other one is induced by the magnetization $\mathbf{M}:\mathbb{R}^d\times(0,T)\to\mathbb{R}^d$ of the nanoparticles. In good approximation the applied magnetic field is not affected by the magnetization of the particles (A3). The magnetic field $\mathbf{H}$ is thus given by the applied magnetic field.

In MPI the applied magnetic field is composed by a static magnetic field $\mathbf{H}_\mathrm{S}:\mathbb{R}^d\to\mathbb{R}^d$, the selection field, and a dynamic magnetic field $\mathbf{H}_\mathrm{D}:(0,T)\to\mathbb{R}^d$, the drive field. The resulting field is their superposition, i.e.,

$$\mathbf{H}(\mathbf{x},t)=\mathbf{H}_\mathrm{S}(\mathbf{x})+\mathbf{H}_\mathrm{D}(t). \tag{4}$$

The selection field is assumed to be a linear function which fulfills $\nabla_\mathbf{x}\cdot\mathbf{H}_\mathrm{S}=0$ for $d=3$ and has full rank (A4). Its transformation matrix is given by $\mathbf{G}_\mathrm{S}\in\mathbb{R}^{d\times d}$. Note that the drive field may also depend on the space variable $\mathbf{x}$ due to the coil sensitivities of the drive field coils. Assuming homogeneous coil sensitivities results in a drive field solely depending on the time variable (A5). With $\mathbf{H}_\mathrm{D}\in(C^1((0,T)))^d$ the implicit function theorem yields that a unique function $\mathbf{p}\in(C^1((0,T)))^d$ exists such that

$$\mathbf{H}(\mathbf{p}(t),t)=0. \tag{5}$$

The function $\mathbf{p}$ is the trajectory of the field free point and is given by

$$\mathbf{p}(t)=\mathbf{H}_\mathrm{S}^{-1}(-\mathbf{H}_\mathrm{D}(t)) \tag{6}$$

such that the magnetic field can be represented in terms of the trajectory of the FFP, i.e.,

$$\mathbf{H}(x,t)=\mathbf{H}_\mathrm{S}(\mathbf{x})-\mathbf{H}_\mathrm{S}(\mathbf{p}(t))=\mathbf{H}_\mathrm{S}(\mathbf{x}-\mathbf{p}(t)). \tag{7}$$

Imaging methodologies are characterized by the trajectory function $\mathbf{p}$, e.g., Cartesian or Lissajous-type trajectories.

The particle behavior is affected by the applied magnetic field. In particular, the change of the particle's magnetization is caused by the dynamics of the applied magnetic field. Common modeling approaches for imaging are based on the assumption that the temporal changes of the magnetic field are sufficiently slow. For this case the mean magnetic moment vector of the particles is assumed to be aligned with the magnetic field vector. Furthermore, nonlinear dependencies on the particle concentration which may be caused by particle-particle interactions are assumed to be negligible. These assumptions justify using the theory of paramagnetism to model the magnetization (A6). The magnetization is then given by

$$\mathbf{M}(\mathbf{x},t)=c(\mathbf{x})\underbrace{\mathscr{L}_{\alpha,\beta}(\|\mathbf{H}(\mathbf{x},t)\|_2)\frac{\mathbf{H}(\mathbf{x},t)}{\|\mathbf{H}(\mathbf{x},t)\|_2}}_{:=\bar{\mathbf{m}}(\mathbf{H}(\mathbf{x},t))} \tag{8}$$

with $\bar{\mathbf{m}}:\mathbb{R}^d\to\mathbb{R}^d$ and the parametrized Langevin function $\mathscr{L}_{\alpha,\beta}:\mathbb{R}\to\mathbb{R}$ defined by

$$\mathscr{L}_{\alpha,\beta}(z)=\alpha\coth(\alpha\beta z)-\frac{1}{\beta z} \tag{9}$$

with physical parameters $\alpha,\beta>0$. They are determined by the saturation magnetization M_core of the core material, the volume of the core V_core, the temperature T, and the Boltzmann constant κ_B, i.e., $\alpha=M_\mathrm{core}V_\mathrm{core}$ and $\beta=\mu_0/(\kappa_\mathrm{B}T)$.

Using the applied magnetic field from Eq. (7) and the magnetization from Eq. (8), Eq. (3) becomes

$$\mathbf{\Phi}(t)=\mathbf{\Psi}_\mathrm{P}(\mathbf{p}(t))+\mathbf{\Psi}_\mathrm{E}(\mathbf{p}(t)) \tag{10}$$

with contributions from particle and excitation signal $\mathbf{\Psi}_\mathrm{P},\mathbf{\Psi}_\mathrm{E}:\mathbb{R}^d\to\mathbb{R}^L$ given by

$$\mathbf{\Psi}_\mathrm{P}(\mathbf{z})=\mu_0\int_{\mathbb{R}^d}\mathbf{p}_\mathrm{R}(\mathbf{x})^Tc(\mathbf{x})\bar{\mathbf{m}}(\mathbf{H}_\mathrm{S}(\mathbf{x}-\mathbf{z}))\,d\mathbf{x},\ \text{and} \tag{11}$$

$$\mathbf{\Psi}_\mathrm{E}(\mathbf{z})=\mu_0\int_{\mathbb{R}^d}\mathbf{p}_\mathrm{R}(\mathbf{x})^T\mathbf{H}_\mathrm{S}(\mathbf{x}-\mathbf{z})\,d\mathbf{x}. \tag{12}$$

10.18416/ijmpi.2017.1707004

Assumption (A2) on the transfer functions of the analog filters implies that $(-\frac{d}{dt}\Psi_{\mathrm{E};k}(\mathbf{p}(\bullet)) * a_k)$, $k = 1, \dots, L$, are sufficiently small such that they can be neglected.

We additionally assume homogeneous coil sensitivities for all receive coils, i.e., $\mathbf{p}_{\mathrm{R}}(\mathbf{x}) = \chi_\Omega(\mathbf{x})\mathbf{R}$ for a given $\mathbf{R} \in \mathbb{R}^{d\times L}$ and characteristic function χ_Ω (A7). It follows that

$$\mathbf{u}(t) = -\nabla_{\mathbf{z}}\Psi_{\mathrm{P}}(\mathbf{p}(t))^T \frac{d}{dt}\mathbf{p}(t) \tag{13}$$

with $\mathbf{H}_{\mathrm{S}}(\mathbf{x}) = \mathbf{G}_{\mathrm{S}}\mathbf{x}$ and

$$\nabla_{\mathbf{z}}\Psi_{\mathrm{P}}(\mathbf{z})^T = \mu_0 \mathbf{R}^T \int_{\mathbb{R}^d} c(\mathbf{x}) \underbrace{D_{\mathbf{z}}\left(\tilde{\mathbf{m}}(\mathbf{H}_{\mathrm{S}}(\mathbf{x}-\mathbf{z}))\right)}_{=:\boldsymbol{\kappa}(\mathbf{x}-\mathbf{z})} d\mathbf{x} \tag{14}$$

with $\mathrm{supp}(c) \subset \Omega$ and where $\boldsymbol{\kappa}\colon \mathbb{R}^d \to \mathbb{R}^{d\times d}$ is given by

$$\boldsymbol{\kappa}(\mathbf{x}) = \left(\frac{\mathbf{G}_{\mathrm{S}}\mathbf{x}\mathbf{x}^T\mathbf{G}_{\mathrm{S}}^T}{\|\mathbf{G}_{\mathrm{S}}\mathbf{x}\|_2^2} \left(\frac{\mathscr{L}_{\alpha,\beta}(\|\mathbf{G}_{\mathrm{S}}\mathbf{x}\|_2)}{\|\mathbf{G}_{\mathrm{S}}\mathbf{x}\|_2} - \frac{\mathrm{d}}{\mathrm{d}z}\mathscr{L}_{\alpha,\beta}(\|\mathbf{G}_{\mathrm{S}}\mathbf{x}\|_2) \right) - \frac{\mathscr{L}_{\alpha,\beta}(\|\mathbf{G}_{\mathrm{S}}\mathbf{x}\|_2)}{\|\mathbf{G}_{\mathrm{S}}\mathbf{x}\|_2} I_d \right) \mathbf{G}_{\mathrm{S}} \tag{15}$$

with $I_d \in \mathbb{R}^{d\times d}$ being the identity matrix. Based on all previous assumptions, the induced potential from Eq. (2) becomes

$$\mathbf{u}(t) = -\mu_0 \mathbf{R}^T (c * \boldsymbol{\kappa})(\mathbf{p}(t)) \frac{d}{dt}\mathbf{p}(t) \tag{16}$$

where $.*$ denotes a convolution in each matrix entry.

The theoretical review of the model results in the following assumptions which are the basis for the subsequent definition of the MPI forward operator.

Assumption 1. *A1. The concentration function $c : \mathbb{R}^d \to \mathbb{R}_+$ fullfils supp$(c) \subset \Omega$, where $\Omega \subset \mathbb{R}^d$ is an open, connected, and bounded set.*

A2. The analog filters are represented by a temporal convolution with the filter kernels $a_k\colon \mathbb{R} \to \mathbb{R}$ which remove the excitation signal from the induced potential, i.e., $\frac{d}{dt}\Psi_{\mathrm{E};k}(\mathbf{p}(\bullet)) * a_k = 0$, $k = 1, \dots, L$.

A3. The magnetic field is independent of the particle magnetization, i.e., $\mathbf{H}\colon \mathbb{R}^d \times (0,T) \to \mathbb{R}^d$ is given by the applied magnetic field. This means $\mathbf{H}$ is determined by the selection field $\mathbf{H}_{\mathrm{S}}$ and the drive field $\mathbf{H}_{\mathrm{D}}$, cf. A4 / A5. It holds $\mathbf{H} = \mathbf{H}_{\mathrm{S}} + \mathbf{H}_{\mathrm{D}}$.

A4. The selection field $\mathbf{H}_{\mathrm{S}}\colon \mathbb{R}^d \to \mathbb{R}^d$ is linear, fulfills $\nabla \cdot \mathbf{H}_{\mathrm{S}} = 0$ for $d = 3$ and its transformation matrix $\mathbf{G}_{\mathrm{S}} \in \mathbb{R}^{d\times d}$ has full rank. The full rank guarantees the existence of a FFP.

A5. The drive field coils are assumed to have homogeneous coil sensitivities such that $\mathbf{H}_{\mathrm{D}}\colon (0,T) \to \mathbb{R}^d$ is independent of the spatial variable. It is further assumed that $\mathbf{H}_{\mathrm{D}} \in (C^1((0,T)))^d$.

A6. The magnetization vector $\mathbf{M}\colon \mathbb{R}^d \times (0,T) \to \mathbb{R}^d$ follows immediately the magnetic field vector $\mathbf{H}$, i.e., it exists a function $f\colon \mathbb{R}^d \times (0,T) \to \mathbb{R}$ such that $\mathbf{M} = cf\frac{\mathbf{H}}{\|\mathbf{H}\|_2}$ where c is the concentration function. It is assumed that f is based on the Langevin function, i.e., $f(\mathbf{x},t) = \mathscr{L}_{\alpha,\beta}(\|\mathbf{H}(\mathbf{x},t)\|_2)$.

A7. The receive coils have homogeneous coil sensitivities in Ω, i.e., $\mathbf{p}_{\mathrm{R}} : \mathbb{R}^d \to \mathbb{R}^{d\times L}$ is given by $\mathbf{p}_{\mathrm{R}}(\mathbf{x}) = \chi_\Omega(\mathbf{x})\mathbf{R}$ for $\mathbf{R} \in \mathbb{R}^{d\times L}$.

Definition 2. *Let $\Omega \subset \mathbb{R}^d$, $d \in \{1,2,3\}$ be an open, connected, and bounded domain. Let $\mathbf{R} \in \mathbb{R}^{d\times L}$, $L \in \mathbb{N}$, and let $\mathbf{r}_k$ denote the k-th column of $\mathbf{R}$. Let $\mathbf{p} \in (C^1(0,T))^d$ with $0 < T < \infty$ and let Assumption 1 be fulfilled. Then the linear MPI forward operator A mapping a concentration function $c\colon \mathbb{R}^d \to \mathbb{R}_+$ to a vector of potential functions $\mathbf{v}\colon (0,T) \to \mathbb{R}^L$ is given by*

$$Ac = \mu_0 \left(\left(\mathbf{r}_k^T (c * \boldsymbol{\kappa})(\mathbf{p}(\bullet)) \frac{d}{dt}\mathbf{p}(\bullet) \right) * a_k \right)_{k=1,\dots,L} \tag{17}$$

with the matrix kernel

$$\boldsymbol{\kappa}(\mathbf{x}) = \left(\frac{\mathbf{G}_{\mathrm{S}}\mathbf{x}\mathbf{x}^T\mathbf{G}_{\mathrm{S}}^T}{\|\mathbf{G}_{\mathrm{S}}\mathbf{x}\|_2^2} \left(\frac{\mathscr{L}_{\alpha,\beta}(\|\mathbf{G}_{\mathrm{S}}\mathbf{x}\|_2)}{\|\mathbf{G}_{\mathrm{S}}\mathbf{x}\|_2} - \frac{\mathrm{d}}{\mathrm{d}z}\mathscr{L}_{\alpha,\beta}(\|\mathbf{G}_{\mathrm{S}}\mathbf{x}\|_2) \right) - \frac{\mathscr{L}_{\alpha,\beta}(\|\mathbf{G}_{\mathrm{S}}\mathbf{x}\|_2)}{\|\mathbf{G}_{\mathrm{S}}\mathbf{x}\|_2} I_d \right) \mathbf{G}_{\mathrm{S}} \tag{18}$$

and $.*$ denoting a convolution in each matrix entry.

This operator is defined as spatial convolutions of the concentration function and the entries of a matrix kernel which is sampled along the FFP trajectory. A linear combination of convolutions with time-dependent weights given by the time derivative of the trajectory then determines the measured potential function. The data acquisition is thus defined by the trajectory $\mathbf{p}$. The degrees of freedom used for the FFP trajectory allows a classification of the reconstruction methods in the MPI literature. Using one degree of freedom corresponds to a Cartesian trajectory. The problem can then be formulated by a single spatial convolution. Using more degrees of freedom for one single trajectory includes the case of Lissajous trajectories. As stated before the latter case obeys a complex structure of the system matrix. This is caused by a temporal change of the linear combination of spatial convolutions.

II.II. Discrete problem

Let the concentration function $c\colon \mathbb{R}^d \to \mathbb{R}_+$, $\mathrm{supp}(c) \subset \Omega$, be an element of a suitable function space X. For the discretization of the problem we assume a given basis $\{\phi_i\}_{i=1,\dots,N_{\mathrm{K}}} \subset X$, $N_{\mathrm{K}} \in \mathbb{N}$, of a finite-dimensional subspace $X_{N_{\mathrm{K}}} \subset X$. From the application point of view, piecewise constant functions are a reasonable

assumption for these basis functions as they may represent pixels or voxels of the concentration image. A concentration function is then given by $c = \sum_{i=1}^{N_\mathrm{K}} c_i \phi_i$. Let $\{t_i\}_{i=1,\dots,N_\mathrm{T}}$ with $t_i = (i-1)T/(N_\mathrm{T}-1)$ be the sequence of equidistant sampling points in time. Inserting both and using a quadrature rule we obtain the discretized system operator

$$S_{\mathrm{model},k} = ((A\phi_j)_k(t_i))_{i=1,\dots,N_\mathrm{T};j=1,\dots,N_\mathrm{K}} \tag{19}$$

for the k-th receive coil. Here we assume that ϕ_j, $j = 1,\dots,N_\mathrm{K}$, are piecewise constant functions on equisized, pairwise disjoint cubic domains. The discretized system operator is obtained by using a 3-point Gauss-Legendre quadrature rule for each space dimension. However due to the analog filter process in the signal acquisition chain, the MPI reconstruction problem is formulated in frequency space by computing the discrete Fourier transform of the time signal. The Fourier transform of the system matrix is denoted by $\widehat{S}_{\mathrm{model},k} \in \mathbb{C}^{N_\mathrm{F}\times N_\mathrm{K}}$, $N_\mathrm{F} \in \mathbb{N}$, in the following.

For given measurements $v_k \in \mathbb{R}^{N_\mathrm{T}}$ the discretized MPI problem then becomes finding $c \in \mathbb{R}_+^{N_\mathrm{K}}$ such that

$$\widehat{S}_{\mathrm{model},k} c = \widehat{v_k} \tag{20}$$

for all $k = 1,\dots,L$. In contrast, the data-based linear problem is formulated by a measured system matrix. In this case the piecewise constant functions $\{\phi_i\}_{i=1,\dots,N_\mathrm{K}}$ represent a "delta" probe which is moved over the entire region Ω [13]. The measured system matrices $S_{\mathrm{data},k}$, $k = 1,\dots,L$, respectively their columns, are then determined by the measured potentials for each basis function ϕ_i, $i = 1,\dots,N_\mathrm{K}$. Analogously to the model-based system function, the Fourier transform with respect to the time variable is denoted by $\widehat{S}_{\mathrm{data},k}$, $k = 1,\dots,L$.

II.III. Transfer function

To determine the transfer functions of the analog filters $a_k : \mathbb{R} \to \mathbb{R}$, $k = 1,\dots,L$, we follow the approach presented in [12]. Given $N \in \mathbb{N}$ tuples of concentrations and potential measurements $(c^{(i)}, v_k^{(i)}) \in \mathbb{R}^{N_\mathrm{K}} \times \mathbb{R}^{N_\mathrm{T}}$ for each receive coil, the j-th Fourier coefficient $\widehat{a_{k,j}}$ of the transfer function is determined by

$$\begin{aligned}\widehat{a_{k,j}} &= \arg\min_{a\in\mathbb{C}} \sum_{i=1}^{N} \|\widehat{v_{k,j}^{(i)}} - a(\widehat{S}_{\mathrm{model},k} c^{(i)})_j\|^2 \\ &= \frac{\sum_{i=1}^{N} \widehat{v_{k,j}^{(i)}} \overline{(\widehat{S}_{\mathrm{model},k} c^{(i)})_j}}{\sum_{i=1}^{N} |(\widehat{S}_{\mathrm{model},k} c^{(i)})_j|^2}.\end{aligned} \tag{21}$$

Here, only data tuples with tracer concentration located in the field of view of the drive field were used.

II.IV. Sparse reconstruction

In MPI the reconstruction of the concentration is often obtained by minimizing a Tikhonov functional with an l^2-penalty term. One of the main drawbacks of this standard approach is that large regularization parameters cause overly smooth reconstructions of the concentration. Including more sophisticated regularization approaches, respectively a priori information, can improve the reconstruction of the concentration which was recently shown by using a fused lasso regularization [23].

We assume that the solution of the problem is sparse in the given basis $\{\phi_i\}_{i=1,\dots,N_\mathrm{K}}$, i.e., the coefficient vector c is sparse. A sparse solution $c \in \mathbb{R}_+^{N_\mathrm{K}}$ is obtained from weighted measurements $v_k \in \mathbb{R}^{N_\mathrm{T}}$, $k = 1,\dots,L$, by minimizing the following Tikhonov type functional

$$J_\gamma(c) = \frac{1}{2}\sum_{k=1}^{L} \|W_{\mathrm{model},k}\widehat{S}_{\mathrm{model},k} c - \widehat{v_k}\|^2 + \gamma\|c\|_1 \tag{22}$$

where $\gamma > 0$ weights the data fidelity term with respect to the l^1-penalty term. Following the approach in [18], the modeled system matrix is weighted with respect to the row energy of the system matrix, i.e., $W_{\mathrm{model},k} \in \mathbb{R}^{N_\mathrm{F}\times N_\mathrm{F}}$ is a diagonal matrix with $1/W_{\mathrm{model},k;i,i} = \sqrt{\sum_{j=1}^{N_\mathrm{K}} |(\widehat{S}_{\mathrm{model},k})_{i,j}|^2}$, $i = 1,\dots,N_\mathrm{F}$. Analogously, we weight the measured data using $W_{\mathrm{data};k} \in \mathbb{R}^{N_\mathrm{F}\times N_\mathrm{F}}$, $k = 1,\dots,L$, obtained from a measured system matrix. This weighting potentially reduces the influence of systematic artifacts not captured by the model. The functional J_γ is minimized by using an iterated soft shrinkage algorithm [25, 30], where the concentration vector is projected by $P_{\mathbb{R}_+^{\mathrm{N}_K}}$ onto the convex set of nonnegative real-valued vectors in each iteration. Considering the concatenated weighted system matrices $\hat{S} \in \mathbb{C}^{LN_\mathrm{F}\times N_\mathrm{K}}$ and concatenated weighted measurements $\hat{v} \in \mathbb{C}^{LN_\mathrm{F}}$ of all receive coils, the iteration becomes

$$c^{i+1} = P_{\mathbb{R}_+^{\mathrm{N}_K}}(g_{\gamma\tau}(c^i - \tau\hat{S}^*(\hat{S}c^i - \hat{v}))) \tag{23}$$

where $g_\delta : \mathbb{C}^{\mathrm{N}_K} \to \mathbb{C}^{\mathrm{N}_K}$, $\delta \geq 0$, is the soft shrinkage operator

$$g_\delta(x) = \left(\begin{cases} \frac{x_i}{|x_i|}(|x_i| - \delta) & \text{if } |x_i| \geq \delta \\ 0 & \text{else.} \end{cases}\right)_{i=1,\dots,\mathrm{N}_K}. \tag{24}$$

In each iteration the step size τ is decreased geometrically until a weak monotonicity criterion is fulfilled. For a detailed description we refer to the algorithm in [31, 32] which has been adapted to the linear case.

II.V. Total least squares with sparsity

Minimizing the functional J_γ in Eq. (22) implicitly assumes noise solely in the measurements. Because of the

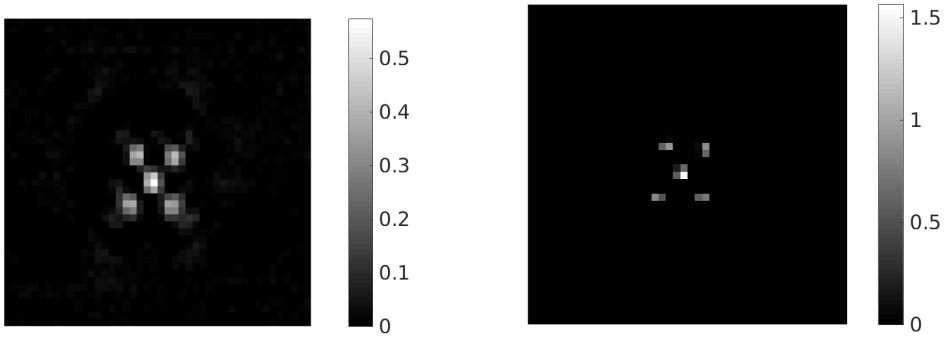

(a) Tikhonov reconstruction, $\gamma = 0.1 \times 10^{-6}$

(b) Sparse reconstruction, $\gamma = 0.1 \times 10^{0}$

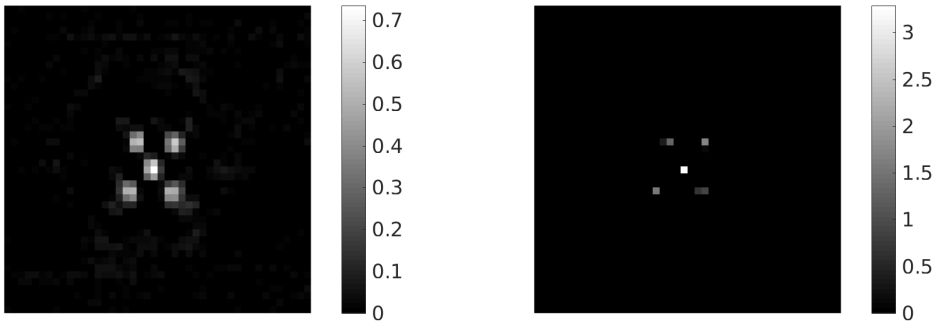

(c) Tikhonov & TLS reconstruction, $\gamma = 0.1 \times 10^{-6}$

(d) Sparse & TLS reconstruction, $\gamma = 0.1 \times 10^{0}$

Figure 1: Data-based reconstructions of the concentration of a 5 point phantom provided by [33]. Reconstructions are obtained without TLS (a,b) and with TLS (c,d) for Tikhonov regularization (a,c) and for sparsity regularization (b,d).

potential model errors and the noise level in measured system matrices, it is reasonable to allow for deviations in the system matrix during the reconstruction process. The following consideration is based on the total least squares approach [27] where an error in the linear operator is assumed. Using the concatenated problem formulation from Sec. II.IV, the extended problem becomes finding the concentration function $c \in \mathbb{R}_+^{N_\mathrm{K}}$ and a deviation matrix $\delta\hat{S} \in \mathbb{C}^{LN_\mathrm{F} \times N_\mathrm{K}}$ which fulfill

$$(\hat{S} + \delta\hat{S})c = \hat{v}. \tag{25}$$

The simultaneous reconstruction of the concentration and the deviation matrix is a nonlinear inverse problem. A solution to the problem is obtained by minimizing the following Tikhonov-type functional

$$J_\gamma^{\mathrm{TLS}}(c, \delta\hat{S}) = \frac{1}{2}\|(\hat{S} + \delta\hat{S})c - \hat{v}\|^2 + \frac{1}{2}\|\delta\hat{S}\|_F^2 + \gamma\|c\|_1 \tag{26}$$

where sparseness of the concentration is assumed and where $\| \bullet \|_F$ denotes the Frobenius norm. The functional is minimized by using an alternating algorithm [34] resulting in the following iteration steps:

$$c^{i+1} = \arg\min_{c \in \mathbb{R}_+^N} J_\gamma^{\mathrm{TLS}}(\delta\hat{S}^i, c) \tag{27}$$

$$\begin{aligned}\delta\hat{S}^{i+1} &= \arg\min_{\delta\hat{S} \in \mathbb{C}^{LN_\mathrm{F} \times N_\mathrm{K}}} J_\gamma^{\mathrm{TLS}}(\delta\hat{S}, c^{i+1}) \\ &= \frac{1}{1 + \|c^{i+1}\|^2}(\hat{v} - \hat{S}c^{i+1})(c^{i+1})^T.\end{aligned} \tag{28}$$

The first step is performed by using the iterated soft shrinkage algorithm from Sec. II.IV. The explicit formulation in the second step results directly from the normal equation.

III. Results

For the numerical tests we use real data without background correction of an FFP scanner provided by the Github project page of [33]. A 2D FFP trajectory is used and data is acquired with three receive coils oriented in x-, y-, and z-direction, i.e., here $d = L = 3$. The measurements are obtained with a cosine excitation with drive field amplitudes of

Parameter		Value
Magnetic permeability	μ_0	$4\pi \times 10^{-7}$ H/m
Boltzmann constant	κ_B	1.38064852 $\times 10^{-23}$ J/K
Temperature	T_{temp}	293 K
Coil sensitivity	$\mathbf{R}$	I_3
Particle diameter	D	30 nm
Sat. magnetization	M_{core}	0.6 T/μ_0
Excitation frequencies	f_x	24.51 kHz
	f_y	26.04 kHz
Excitation amplitudes	A_x	14 mT/μ_0
	A_y	14 mT/μ_0
Gradient strength	G_x	-1.25 T/m/μ_0
	G_y	-1.25 T/m/μ_0
	G_z	2.5 T/m/μ_0

Table 1: Model parameters used for the model-based reconstruction in Fig. 2.

14 mT/μ_0 in both excitation directions and a gradient strength of $G_x = G_y = -1.25$ T/m/μ_0 and accordingly $G_z = 2.5$ T/m/μ_0. The Lissajous measurement circle with a repetition time of $T = 0.6528$ ms is generated by a base frequency of 2.5 MHz and frequency dividers 102 and 96. The size of the field of view is 44 mm $\times$ 44 mm $\times$ 1 mm. The field of view is sampled at $44 \times 44 \times 1 = 1936$ positions such that the system matrix has 1936 columns. The time signals were sampled with 2.5 MHz resulting in $N_T = 1632$ discrete time points. Frequencies larger than 30 kHz and smaller than 1.25 MHz have been used for the reconstruction resulting in a number of 797 rows in the system matrix for each receive coil.

The parameters used for the model-based system matrix are summarized in Tab. 1. With these parameters the selection field $\mathbf{H}_S(\mathbf{x}) = \mathbf{G}_S\mathbf{x}$ is given by the diagonal matrix $\mathbf{G}_S \in \mathbb{R}^{3\times3}$ with the gradient strengths G_x, G_y, and G_z on the diagonal. The drive field is modeled by $\mathbf{H}_D(t) = (A_x \cos(f_x t 2\pi), -A_y \cos(f_y t 2\pi), 0)^T$. The measured system function, which is also provided by [33], is used to compute the transfer functions $\hat{a_k}$, $k = 1, 2, 3$, from $N = 484$ data tuples as described in Sec. II.III. In case of fitting the transfer function it is sufficient to assume unit vectors for the receive coil sensitivities as the value is already included in the fitted transfer function. The iterated soft shrinkage algorithm from Sec. II.IV and the alternating algorithm from Sec. II.V are used to compute reconstructions from the data-based as well as from the model-based approach. The regularization parameters are chosen by visual inspection of the reconstructed images. Equal parameter values are used for the reconstructions with and without considering the deviation in the system matrix.

A five point phantom consisting of glass capillary with a diameter of 1.1 mm filled with Resovist with a concentration of 0.5 mol/l provided by the Github project page of [33] is reconstructed. The nonnegative Tikhonov regularization is computed with the Kaczmarz implementation which is also provided with the data. The reconstructions are computed with one iteration as suggested in the example script of [33].

The data-based reconstructions are shown in Fig. 1. We obtain smoothed reconstructions of the five points which is typical for Tikhonov regularization, cf. Fig. 1(a). In contrast the minimization with sparsity constraints is able to obtain a better localization of the tracer. The difference in concentration values depends strongly on the choice of the regularization parameter. Signal energy from regions filled with tracer which are not included in the used system matrix may cause a larger concentration value than the expected 0.5 mol/l. Using the total least squares approach further improves the localization in the sparse reconstruction for the data-based system matrices, cf. Fig. 1(d). In case of Tikhonov regularization the concentration values increase slightly.

By using the parameters in Tab. 1 and the data-based weighting of the data, we were able to obtain the model-based reconstruction presented in Fig. 2. The ratio between the data-based and the model-based weighting is illustrated in Fig. 3 for all receive coils. For the receive coils in x- and y-direction a much smaller ratio can be found on the higher harmonics of the respective drive field frequency. The smaller the ratio the more is the measured data rescaled in these frequency components. The scaling reduces the influence of artifacts in these frequency components in the reconstruction process.

As can be seen in Fig. 2(a) using Tikhonov regularization results in a reconstruction of the five dots with additional background artifacts. Using the total least squares approach in this setup increases the contrast in concentration values but background artifacts are not reduced. The small number of iterations in the Kaczmarcz algorithm which does not guarantee sufficient convergence and large artifacts in the measurements are possible reasons for the remaining artifacts in the reconstruction. In contrast to the data-based reconstruction with Tikhonov regularization, the sparse model-based reconstruction in Fig. 2(b) has a similar quality in terms of localization of the dots. Furthermore the model-based sparse reconstruction is less smooth. By using the total least squares approach in Fig. 2(d) the localization of the dots can be further improved such that the localization is similar in quality compared to the data-based sparse reconstruction. The loss in contrast might be due to a regularization parameter chosen too large.

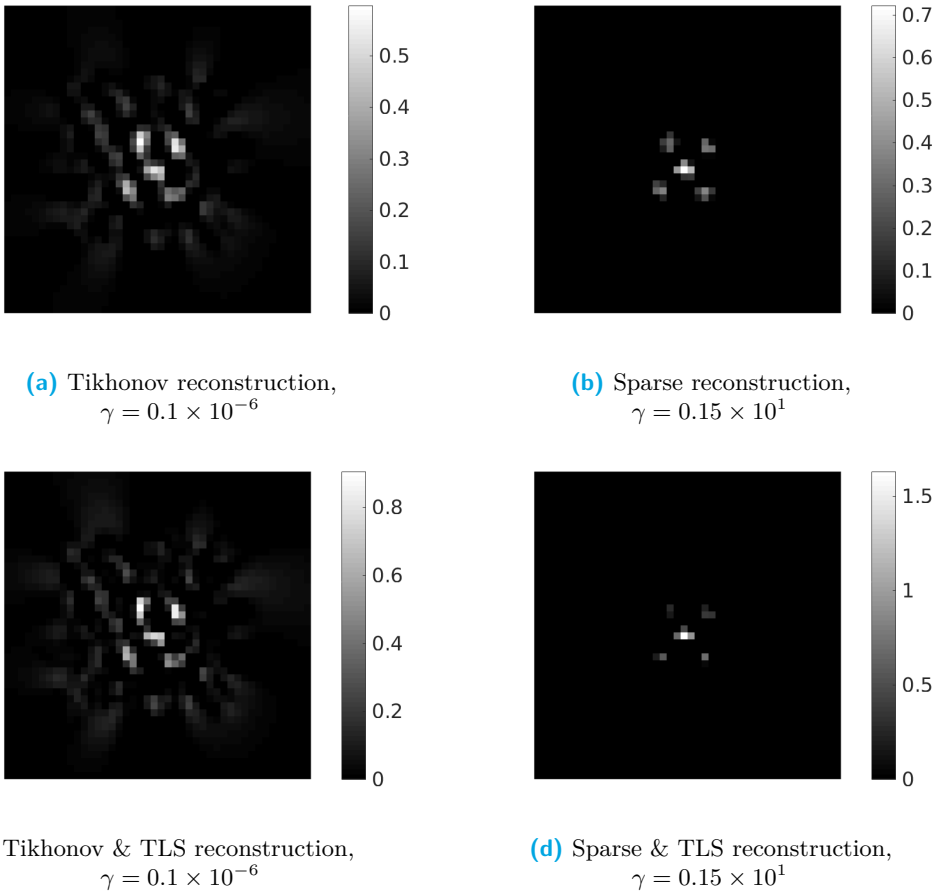

(a) Tikhonov reconstruction, $\gamma = 0.1 \times 10^{-6}$

(b) Sparse reconstruction, $\gamma = 0.15 \times 10^{1}$

(c) Tikhonov & TLS reconstruction, $\gamma = 0.1 \times 10^{-6}$

(d) Sparse & TLS reconstruction, $\gamma = 0.15 \times 10^{1}$

Figure 2: Model-based reconstructions of the concentration of a 5 point phantom provided by [33]. Reconstructions are obtained without TLS (a,b) and with TLS (c,d) for Tikhonov regularization (a,c) and for sparsity regularization (b,d).

IV. Discussion

In the present work we include the additional degree of freedom of model errors which may prevent the use of model-based approaches in MPI. The total least squares investigation is accompanied by the incorporation of sparsity constraints in the reconstruction of the concentration. We are able to reconstruct sparse particle concentrations from real data with data-based and model-based system functions. By incorporating the sparseness assumption, the reconstruction obtained from the data-based and model-based system functions can be improved. The structure of the model-based results look promising in the case of sparse reconstructions. The artifacts in the Tikhonov reconstructions might be due to a systematic behavior of the system which is not covered by the model, e.g., drive field artifacts. The choice of the regularization parameter strongly influences the reconstructed concentration values. Aiming for stable model-based reconstruction techniques which are able to deal with uncertainty to some degree is advantageous for MPI since a sufficient model is still missing.

To obtain a reasonable model-based reconstruction we used fitted transfer functions and a data-based weighting of the data which is critical with respect to the evaluation of the assumed model and the interpretation of the reconstructed system matrix deviations. Transfer functions which are fitted to measured system functions can use the additional degree of freedom to compensate potential drawbacks of the assumed model. As a consequence the implementation of the drive field and/or the assumption (A6) regarding the dynamics of the magnetic moments of the particles may be incorrect. Artifacts in the frequency bands which correspond to higher harmonics of the excitation frequencies are not predicted by the assumed model which can be seen in the ratio of model- and data-based weights. The proposed weighting of the system function may reduce the model error as the influence in the reconstruction is suppressed. This observation raises the question whether assumption (A2) holds strictly true.

The present work is the basis for several directions of research. The model-based approach with sparsity

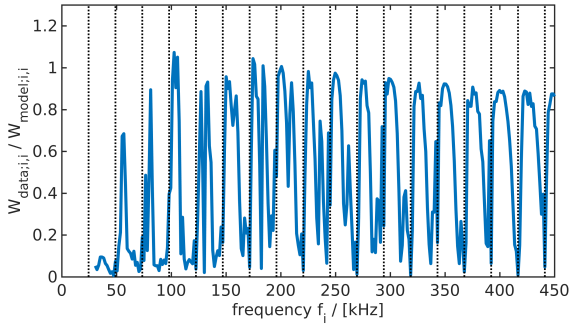

(a) Receive coil x-direction

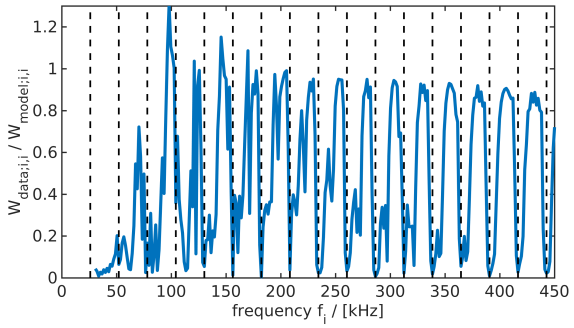

(b) Receive coil y-direction

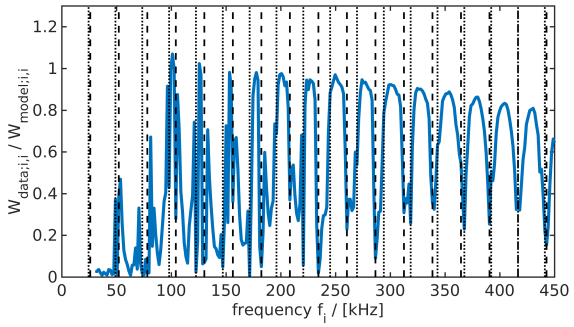

(c) Receive coil z-direction

Figure 3: The ratio between the data-based weights $W_{\text{data},k}$ and the model-based weights $W_{\text{model},k}$, $k = 1, \ldots, 3$, for receive coils in x-, y-, and z-direction are illustrated. Vertical lines highlight higher harmonics of the drive field frequencies f_x (dotted) and f_y (dashed).

constraints and model uncertainty used in this work should be investigated on larger data sets and without fitting the transfer functions of the analog filters in the signal acquisition chain. For this purpose more efficient algorithms for the sparse reconstructions, e.g., FISTA [35], should be incorporated. Another direction of research is the solution of further nonlinear problems aiming for a deeper undersanding of the model errors. For example, considering deviations in the magnetic field vector in the used model might be of interest to identify potentially emerging relaxation effects. The nonlinear nature of these problems requires a theoretical analysis and a subsequent development of efficient solvers as well as the mathematical analysis of the forward operator given by the model. A successful validation of the presented approach would be advantageous for applications in MPI, e.g., imaging blood flow or tracking medical instruments [2–4]. The model-based approach allows further investigation of memory efficient representations of the system operator [36, 37] particularly for three-dimensional imaging applications.

Acknowldegement

The authors would like to thank T. Knopp for introducing them to MPI and for many valuable advices and fruitful discussions. T. Kluth is supported by the Deutsche Forschungsgemeinschaft (DFG) within the framework of GRK 2224/1 “Pi^3: Parameter Identification - Analysis, Algorithms, Applications”. P. Maass acknowledges funding from the German Federal Ministry of Education and Research (BMBF, project no. 05M16LBA).

References

[1] B. Gleich and J. Weizenecker. Tomographic imaging using the nonlinear response of magnetic particles. *Nature*, 435 (7046):1214–1217, 2005. doi:10.1038/nature03808.

[2] J. Weizenecker, B. Gleich, J. Rahmer, H. Dahnke, and J. Borgert. Three-dimensional real-time in vivo magnetic particle imaging. *Phys. Med. Biol.*, 54(5):L1–L10, 2009.

[3] J. Haegele, J. Rahmer, B. Gleich, J. Borgert, H. Wojtczyk, N. Panagiotopoulos, T. M. Buzug, J. Barkhausen, and F. M. Vogt. Magnetic Particle Imaging: Visualization of Instruments for Cardiovascular Intervention. *Radiology*, 265 (3):933–938, 2012.

[4] J. Salamon, M. Hofmann, C. Jung, M. G. Kaul, F. Werner, K. Them, R. Reimer, P. Nielsen, A. vom Scheidt, G. Adam, T. Knopp, and H. Ittrich. Magnetic Particle / Magnetic Resonance Imaging: In-Vitro MPI-Guided Real Time Catheter Tracking and 4D Angioplasty Using a Road Map and Blood Pool Tracer Approach. *PLOS ONE*, 11(6):e0156899, 2016. doi:10.1371/journal.pone.0156899.

[5] N. Löwa, P. Radon, O. Kosch, and F. Wiekhorst. Concentration Dependent MPI Tracer Performance. *Intern. J. Magnetic Particle Imaging*, 2(1):1601001, 2016. doi:10.18416/ijmpi.2016.1601001.

[6] Thomas März and Andreas Weinmann. Model-based reconstruction for magnetic particle imaging in 2D and 3D. *Inverse Problems and Imaging*, 10(4):1087–1110, 2016. doi:10.3934/ipi.2016033.

[7] J. Rahmer, J. Weizenecker, B. Gleich, and J. Borgert. Signal encoding in magnetic particle imaging: properties of the system function. *BMC Medical Imaging*, 9(4), 2009. doi:10.1186/1471-2342-9-4.

[8] P. W. Goodwill and S. M. Conolly. The x-Space Formulation of the Magnetic Particle Imaging process: One-Dimensional Signal, Resolution, Bandwidth, SNR, SAR, and Magne-

tostimulation. *IEEE Trans. Med. Imag.*, 29(11):1851–1859, 2010. doi:10.1109/TMI.2010.2052284.

[9] T. Knopp, S. Biederer, T. F. Sattel, J. Rahmer, J. Weizenecker, B. Gleich, J. Borgert, and T. M. Buzug. 2D model-based reconstruction for magnetic particle imaging. *Med. Phys.*, 37(2):485–491, 2010. doi:10.1118/1.3271258.

[10] L. R. Croft, P. W. Goodwill, and S. M. Conolly. Relaxation in X-Space Magnetic Particle Imaging. *IEEE Trans. Med. Imag.*, 31(12):2335–2342, 2012. doi:10.1109/TMI.2012.2217979.

[11] M. Graeser, K. Bente, A. Neumann, and T. M. Buzug. Trajectory dependent particle response for anisotropic mono domain particles in magnetic particle imaging. *Journal of Physics D: Applied Physics*, 49(4):045007, 2015. doi:10.1088/0022-3727/49/4/045007.

[12] T. Knopp, T. F. Sattel, S. Biederer, J. Rahmer, J. Weizenecker, B. Gleich, J. Borgert, and T. M. Buzug. Model-Based Reconstruction for Magnetic Particle Imaging. *IEEE Trans. Med. Imag.*, 29(1):12–18, 2010. doi:10.1109/TMI.2009.2021612.

[13] M. Grüttner, T. Knopp, J. Franke, M. Heidenreich, J. Rahmer, A. Halkola, C. Kaethner, J. Borgert, and T. M. Buzug. On the formulation of the image reconstruction problem in magnetic particle imaging. *Biomed. Tech. / Biomed. Eng.*, 58(6):583–591, 2013. doi:10.1515/bmt-2012-0063.

[14] J. J. Konkle, P. W. Goodwill, D. W. Hensley, R. D. Orendorff, M. Lustig, and S. M. Conolly. A Convex Formulation for Magnetic Particle Imaging X-Space Reconstruction. *PLOS ONE*, 10(10):e0140137, 2015. doi:10.1371/journal.pone.0140137.

[15] B. Zheng, T. Vazin, P. W. Goodwill, A. Conway, A. Verma, E. U. Saritas, D. Schaffer, and S. M. Conolly. Magnetic Particle Imaging tracks the long-term fate of in vivo neural cell implants with high image contrast. *Sci. Rep.*, 5:14055, 2015. doi:10.1038/srep14055.

[16] P. W. Goodwill and S. M. Conolly. Multidimensional X-Space Magnetic Particle Imaging. *IEEE Trans. Med. Imag.*, 30(9):1581–1590, 2011. doi:10.1109/TMI.2011.2125982.

[17] T. Knopp, S. Biederer, T. F. Sattel, and T. M. Buzug. Singular value analysis for Magnetic Particle Imaging. In *IEEE Nuclear Science Symposium*, pages 4525–4529, 2008. doi:10.1109/NSSMIC.2008.4774296.

[18] T. Knopp, J. Rahmer, T. F. Sattel, S. Biederer, J. Weizenecker, B. Gleich, J. Borgert, and T. M. Buzug. Weighted iterative reconstruction for magnetic particle imaging. *Phys. Med. Biol.*, 55(6):1577–1589, 2010. doi:10.1088/0031-9155/55/6/003.

[19] J. Rahmer, J. Weizenecker, B. Gleich, and J. Borgert. Analysis of a 3-D System Function Measured for Magnetic Particle Imaging. *IEEE Trans. Med. Imag.*, 31(6):1289–1299, 2012. doi:10.1109/TMI.2012.2188639.

[20] J. Lampe, C. Bassoy, J. Rahmer, J. Weizenecker, H. Voss, B. Gleich, and J. Borgert. Fast reconstruction in magnetic particle imaging. *Phys. Med. Biol.*, 57(4):1113–1134, 2012. doi:10.1088/0031-9155/57/4/1113.

[21] M. G. Kaul, O. Weber, U. Heinen, A. Reitmeier, T. Mummert, C. Jung, N. Raabe, T. Knopp, H. Ittrich, and G. Adam. Combined Preclinical Magnetic Particle Imaging and Magnetic Resonance Imaging: Initial Results in Mice. *Fortschr. Röntgenstr.*, 187(05):347–352, 2015. doi:10.1055/s-0034-1399344.

[22] T. Knopp and M. Hofmann. Online reconstruction of 3D magnetic particle imaging data. *Phys. Med. Biol.*, 61(11): N257–N267, 2016. doi:10.1088/0031-9155/61/11/N257.

[23] M. Storath, C. Brandt, M. Hofmann, T. Knopp, J. Salamon, A. Weber, and A. Weinmann. Edge Preserving and Noise Reducing Reconstruction for Magnetic Particle Imaging. *IEEE Trans. Med. Imag.*, 36(1):74–85, 2017. doi:10.1109/TMI.2016.2593954.

[24] C. Bathke, T. Kluth, C. Brandt, and P. Maass. International Journal on Magnetic Particle ImagingVol 3, No 1, Article ID 1703015, 10 PagesResearch ArticleImproved Image Reconstruction in Magnetic Particle Imaging using Structural a priori Information. *Intern. J. Magnetic Particle Imaging*, 3(1):1703015, 2017. doi:10.18416/ijmpi.2017.1703015.

[25] B. Jin and P. Maass. Sparsity regularization for parameter identification problems. *Inverse Probl.*, 28(12):123001, 2012. doi:10.1088/0266-5611/28/12/123001.

[26] L. I. Rudin, S. Osher, and E. Fatemi. Nonlinear total variation based noise removal algorithms. *Physica D*, 60(1): 259–268, 1992. doi:10.1016/0167-2789(92)90242-F.

[27] G. H. Golub, P. C. Hansen, and D. P. O'Leary. Tikhonov regularization and total least squares. *SIAM. J. Matrix Anal. & Appl.*, 21(1):185–194, 1999. doi:10.1137/S0895479897326432.

[28] H. Schomberg. Magnetic particle imaging: Model and reconstruction. In *IEEE International Symposium on Biomedical Imaging: From Nano to Macro*, pages 992–995, 2010. doi:10.1109/ISBI.2010.5490155.

[29] T. Knopp and T. M. Buzug. *Magnetic Particle Imaging: An Introduction to Imaging Principles and Scanner Instrumentation*. Springer, Berlin/Heidelberg, 2012. doi:10.1007/978-3-642-04199-0.

[30] I. Daubechies, M. Defrise, and C. De Mol. An Iterative Thresholding Algorithm for Linear Inverse Problems with a Sparsity Constraint. *Comm. Pure Appl. Math.*, 57(11): 1413–1457, 2004. doi:10.1002/cpa.20042.

[31] M. Gehre, T. Kluth, A. Lipponen, B. Jin, A. Seppänen, J. P. Kaipio, and P. Maass. Sparsity reconstruction in electrical impedance tomography: an experimental evaluation. *J. Comput. Appl. Math.*, 236(8):2126–2136, 2012. doi:10.1016/j.cam.2011.09.035.

[32] M. Gehre, T. Kluth, C. Sebu, and P. Maass. Sparse 3D reconstructions in electrical impedance tomography using real data. *Inverse Probl. Sci. Eng.*, 22(1):31–44, 2014. doi:10.1080/17415977.2013.827183.

[33] T. Knopp, T. Viereck, G. Bringout, M. Ahlborg, J. Rahmer, and M. Hofmann. MDF: Magnetic Particle Imaging Data Format. *arXiv:1602.06072 [physics.med-ph]*, 2016.

[34] H. Zhu, G. Leus, and G. B. Giannakis. Sparsity-cognizant total least-squares for perturbed compressive sampling. *IEEE Trans. Signal Process.*, 59(5):2002–2016, 2011. doi:10.1109/TSP.2011.2109956.

[35] A. Beck and M. Teboulle. A Fast Iterative Shrinkage-Thresholding Algorithm for Linear Inverse Problems. *SIAM J. Imaging Sci.*, 2(1):183–202, 2009. doi:10.1137/080716542.

[36] T. Knopp and A. Weber. Local System Matrix Compression for Efficient Reconstruction in Magnetic Particle Imaging. *Adv. Math. Phys.*, 2015(472818), 2015. doi:10.1155/2015/472818.

[37] A. Weber and T. Knopp. Reconstruction of the Magnetic Particle Imaging System Matrix Using Symmetries and Compressed Sensing. *Adv. Math. Phys.*, 2015:460496, 2015. doi:10.1155/2015/460496.

